

## Finite Orbit Width Features in the CQL3D Code

Yu. V. Petrov, R. W. Harvey

CompX, Del Mar, CA 92014, USA

*E-mail contact of main author: petrov@compcco.com*

**Abstract.** The CQL3D Fokker-Planck equation solver is being upgraded to allow for the Finite-Orbit-Width (FOW) capabilities, which will provide an accurate description for a neoclassical transport, losses to the walls, and transfer of particles, momentum, and heat to the scrape-off layer. Two different options are discussed for implementing the FOW capabilities. In one option, the Fokker-Planck equation is solved for the distribution function of orbits centered around given flux surface; in the other, the equation is solved for the local distribution function at the grid points along the midplane. Both options use a fast lookup table that allows characterization of orbits without actually tracing them. The lookup table, in effect, performs mapping from the Constants-Of-Motion space onto the  $(R_0, u_0, \theta_0)$  computational space on the midplane. The FOW modifications have been implemented for the formations of neutral beam source, rf quasilinear diffusion operator, particle diagnostics and collisional operator, and internal boundary conditions are being refined.

### 1. Introduction

The CQL3D Fokker-Planck equation (FPE) solver [1, 2] is widely used in the tokamak physics community because of its versatility. It is a relativistic, multi-species code with the full nonlinear Coulomb collision operator and quasilinear RF diffusion terms for waves in a broad frequency range. It also models a neutral beam source of ions, and is coupled with full

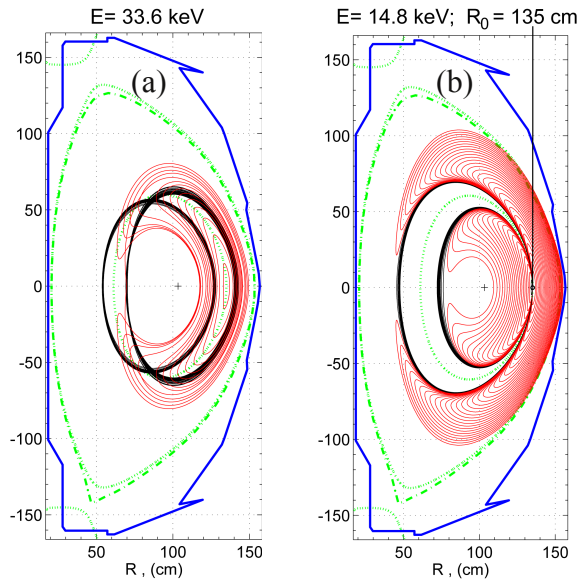


FIG. 1. Two options for introducing FOW effects into CQL3D code: (a) Distribution function of  $D^+$  orbits in NSTX centered around given flux surface; (b) Local distribution function at  $R_0$ .

wave, ray-tracing, and transport codes as part of the SciDAC Integrated Plasma Simulator project. The code is favored by experimentalists because of a large set of synthetic diagnostics tools. Until now CQL3D was using the Zero-Orbit-Width (ZOW) approximation; present work describes the recent modifications in the code to account for the Finite-Orbit-Width (FOW) effects. The FOW capabilities will provide an accurate description for a neoclassical transport, including very important losses to the walls, and transfer of particles, momentum, and heat to the scrape-off layer. For the FOW modifications, two options have been considered, which are illustrated in Fig. 1. In the first option, the distribution function for a given flux surface consists of all orbits that have same value of bounce-average poloidal flux  $\langle \Psi_{pol} \rangle$ , equal to the value of poloidal flux at this surface.

As seen in Fig. 1(a), the trapped orbits (red) representing such distribution are simply centered around the flux surface; the co-passing and counter-passing (both black color) are shifted in opposite direction from the surface. Such distribution function of  $\Psi_{pol}$ -centered orbits is not the local distribution function of particles that would be needed for calculation of current and for synthetic diagnostics; but once the  $\Psi_{pol}$ -centered distribution function is known, the local distribution can be reconstructed at any given  $(R, Z)$  point in cross-section. In the second option, illustrated in Fig. 1(b), the distribution function is actually the local distribution function at point  $R_0$ , the intersection point of the flux surface with the midplane. Hereinafter, the subscript “0” refers to the points on the midplane. Each option has its own advantages and drawbacks. The main advantage of the first option is that it is fast – only twice slower than the original CQL3D-ZOW code. However, only partial FOW capabilities are implemented in this version. The FOW-related modifications are made for the formations of particle source operator (NBI source), RF quasilinear operator, synthetic diagnostics, and the loss cone. Other than that, the collisional operator remains ZOW, which is justified by the fact that each orbit spends approximately equal time on each side of magnetic surface. The Fokker-Planck equation also remains in the ZOW form (except modifications listed above), with same boundary conditions as in the original ZOW FPE. For these reasons, we call this version the Hybrid-FOW model. Because of the ZOW-type FPE, the model lacks neoclassical transport; however, a model radial diffusion can be added into FPE in a same manner as it is done in the ZOW version of the code.

In the second version, which we call Full-FOW, the bounce-averaged FPE is re-written to include all proper transformation coefficients and proper Jacobian, starting from the canonical angle-action space and casting the FPE into the form that is solved over “convenient” computational 3D-grid. As a result, such FPE includes all radial terms that yield neoclassical radial transport. The collisional operator is numerically averaged over each orbit of the 3D-grid. The main complication in this version is the internal boundary conditions (IBC).

## 2. COM mapping table

It should be emphasized that the CQL3D code seeks the solution for the *bounce-averaged* (BA) Fokker-Planck equation, so that the distribution function, whether it's option one or two discussed above, is a function of only three variables – a spatial coordinate ( $\Psi_{pol}$  or  $R_0$ ), the particle speed (momentum/rest-mass)  $u_0$ , and the pitch-angle  $\theta_0$  related to the spatial coordinate. Therefore, all source or sink terms should be expressed in terms of only one spatial coordinate. In the ZOW approximation, this was a trivial task; if, for instance, there is a source of particles at some point  $(R, Z)$ , we only have to find the flux surface that goes through this point and then follow the surface to the midplane to assign all these particles to the coordinate  $R_0$ . With FOW modifications, such particles must be assigned to sources at different midplane coordinates, because the shape of orbits depends on local  $(u, \theta)$ . It is clear that the direct tracing of orbits would enormously increase the computation time. To address this problem, a fast lookup table procedure has been developed that allows a nearly immediate characterization of orbits. It can be used for both options discussed above. The lookup table, in effect, performs mapping from the Constants-Of-Motion (COM) space onto the  $(R_0, u_0, \theta_0)$  space on the midplane [3], where the grids are defined. The COM table is generated in the beginning of each run; it uses uniform grid in adiabatic invariant  $\mu$  and canonical angular momentum  $p_\phi$ , and generally non-uniform grid in particle speed  $u$  (to be replaced by total energy, when the radial electric field is added). Thus, the COM table is generated as a

function of  $(u, \mu, p_\phi)$ -indices,  $(i_u, i_\mu, i_{p_\phi})$ . The table contains values for the radial coordinates of orbit legs on the midplane, corresponding pitch-angles, and the values of  $\Psi_{pol}$  at the legs' coordinates. Besides, the values of bounce-average  $\langle \Psi_{pol} \rangle$  and bounce time  $\tau_b$  are found and stored by tracing the g.c. orbits for each grid triplet  $(i_u, i_\mu, i_{p_\phi})$ . The whole calculation for generating the table and tracing all orbits takes  $\sim 5$  min on a single CPU. The usage of the table for the formation of the particle source operator is as follows: (1). For each particle “born” at point  $(R, Z)$  in plasma cross-section, with local  $(u, \theta)$ , evaluate  $p_\phi$  and  $\mu$ . (2). Find the nearest triplet index  $(i_u, i_\mu, i_{p_\phi})$  in the corresponding grids of  $(u, \mu, p_\phi)$ . (3). Call the table. A logical branching based on the sign of the local  $\cos\theta$  is used to identify the proper orbit (up to two orbits may exist for a given  $(i_u, i_\mu, i_{p_\phi})$ ). In the Hybrid-FOW version, the particle is assigned to the flux surface nearest to  $\langle \Psi_{pol} \rangle$  found from the table. In the full-FOW version, the particle is assigned to position of orbit legs on the midplane. Thus, the source is formed in terms of the midplane computational coordinates in which the Fokker-Plank equation is to be solved.

A similar procedure is applied for the formation of the RF quasilinear diffusion operator (example for hybrid-FOW): Consider a ray element at the local point  $(R, Z)$ . Set a local grid over the resonance region in local  $(u_\parallel, u_\perp)$ -space (vertical strip for ICRH case). For each local  $(u_\parallel, u_\perp)$ -point from the resonance region, find the value of  $\langle \Psi_{pol} \rangle$  from the COM table; then, determine the nearest grid-surface  $\rho_0$  and corresponding midplane value of pitch angle  $\theta_0$ . The power from the ray element is assigned to the quasilinear coefficient at this  $(\rho_0, u_0, \theta_0)$ . It is seen that in FOW, the ray-element power is “spread” over many surfaces. Hence, a broader profile of current density, comparing to ZOW.

The table is also used for the formation of the loss cone. The g.c. orbits are traced for every  $(i_u, i_\mu, i_{p_\phi})$ -index in the table: If the orbit + gyro-radius hits the wall (outside of LCFS), the particle is considered lost.

### 3. Application of the Hybrid-FOW version

As noted above, the distribution function found at  $R_0(l_R)$  radial grid point as a solution of the Hybrid-FOW model, is not a local distribution function. It is rather the distribution function for particles with given BA radial position, none of which passes through  $R_0$ , except the stagnation orbits. We designate it as  $f_{\langle \Psi \rangle}(R_0, u_0, \theta_0)$ . However, once such solution is obtained, the local distribution  $f_{loc}(R, Z, u, \theta)$  can be reconstructed at any given  $(R, Z)$  point in cross-section, including points along

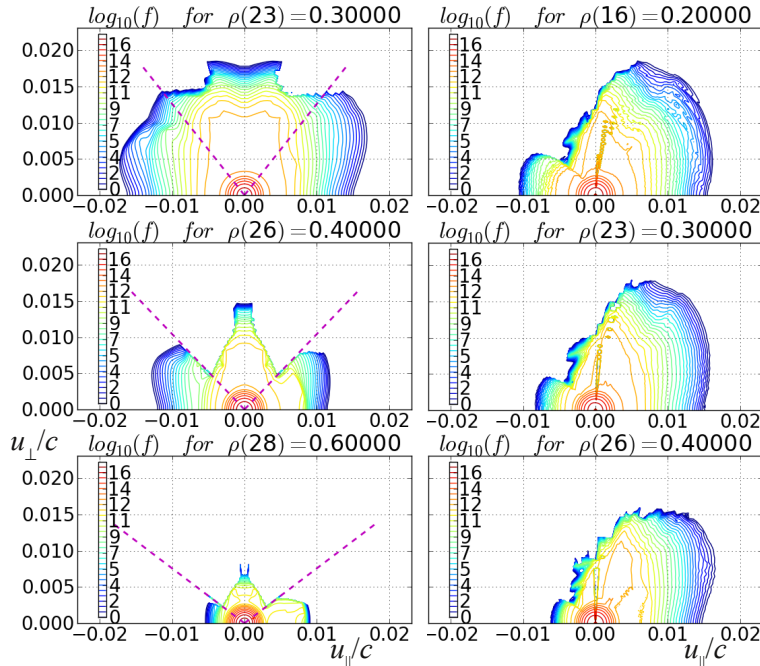


FIG. 2. Left column: Distribution function  $f_{\langle \Psi \rangle}$  as a solution of the Hybrid-FOW version. Right column: Reconstructed local distribution function at different midplane points. NSTX plasma with NBI and RF heating.

the midplane, by using the COM table. The example of reconstructed local distribution is shown in Fig. 2. The orbits with  $\theta_0 < \pi/2$  come from smaller (inner) flux surfaces, and they are well confined; the orbits with  $\theta_0 > \pi/2$  come from larger outer flux surfaces, many of such orbits are lost to the wall (orbit-position + gyro-radius).

For synthetic diagnostics, the local distribution functions are reconstructed along sight lines. Typically, only the high-energy part of the distribution,  $E > 30$  keV, is required for diagnostics. As seen in Fig. 1, the FOW effects are already significant for such particles. As an example, when the FOW effects were ignored in the CQL3D-ZOW calculations of Fast Ion Diagnostics (FIDA) in NSTX, the predicted spatial profiles were shifted towards magnetic axis, comparing to the measured signal [4]. In contrast, application of the Hybrid-FOW version yields an almost perfect match of the simulated FIDA profile with experimental data, in terms of the peak position and magnitude [5].

#### 4. Development of the Full-FOW version

The initial approach for the derivation of the bounce-averaged FPE has been developed in [6, 7]. The main idea is that the original 6D kinetic equation can be first written in canonical action-angle space, and then it can be averaged over periodic angle variables, therefore reducing the dimensionality to 3D. Such averaging is justified by assumptions of toroidally symmetric magnetic geometry, bounce time  $\tau_b$  of charged particles being much less than the collision time, and small gyroradius. However, the remaining three variables (action variables) are not suitable for numerical coding. Therefore the next step is to substitute the canonical action variables by a new set of invariants  $\mathbf{I} = (I_1, I_2, I_3)$  that define finite-orbit-width motion in symmetric torii and which are better suited for numerical grids [8, 9, 10]. Such substitution results in a general shape of the bounce-averaged Fokker-Planck equation for the particle distribution function  $f_0$ :

$$\frac{\partial}{\partial t} J f_0(\mathbf{I}, t) = \frac{\partial}{\partial I_i} J \left[ D^{ij} \frac{\partial}{\partial I_j} - F^i \right] f_0(\mathbf{I}, t)$$

where summation convention is used. The Jacobian,  $J$ , is such that  $f_0$  is the number of particles in the volume element  $J d^3 \mathbf{I}$ . The bounce-averaged diffusion coefficient and friction terms resulting from the local collisional diffusion are thus given by

$$D^{ij} = \left\langle \frac{\partial I_i}{\partial \mathbf{u}} \mathbf{D}^{uu} \frac{\partial I_j}{\partial \mathbf{u}} \right\rangle \quad \text{and} \quad F^i = \left\langle \frac{\partial I_i}{\partial \mathbf{u}} \cdot \mathbf{F}^u \right\rangle$$

where the tensor  $\mathbf{D}^{uu}$  and vector  $\mathbf{F}^u$  are the local collisional plus QL RF diffusion coefficients and the collisional friction, respectively. The brackets  $\langle \dots \rangle$  indicate a bounce average along the g.c. orbit defined by the COM. Note that Coulomb collisions and RF QL diffusion are a spatially local phenomena, changing only a particles velocity  $\mathbf{u}$ , not position. Similarly, the bounce-averaged toroidal electric field gives rise to the term

$$F_T^i = \left\langle \frac{-q}{m} E_T \frac{\partial I_i}{\partial \mathbf{u}} \cdot \mathbf{e}_\phi \right\rangle.$$

A particular form of the FPE depends on the choice of  $\mathbf{I} = (I_1, I_2, I_3)$  space. Since all particles can be assumed to pass through the torus equatorial midplane (or equivalently the ‘‘stagnation’’ surface [3] in the non-up-down symmetric case), we can take the constants of motion to be  $(I_1, I_2, I_3) = (u_0, \theta_0, R_0)$ , the particle speed (or, relativistically, momentum-per-mass), pitch angle from the direction of the magnetic field, and the major radius of the particle

evaluated at the midplane. With this choice, the actual local particle distribution on the equatorial plane is determined. For the selected grid space  $\mathbf{I} = (u_0, \theta_0, R_0)$ , the collisional operator can be written as

$$\begin{aligned} \left( \frac{\partial f}{\partial t} \right)_{coll} &= \frac{1}{\lambda u_0^2} \frac{\partial}{\partial u_0} \left( A f + B \frac{\partial f}{\partial u_0} + C \frac{\partial f}{\partial \theta_0} + R_{13} \frac{\partial f}{\partial R_0} \right) \\ &+ \frac{1}{\lambda u_0^2 \sin \theta_0} \frac{\partial}{\partial \theta_0} \left( D f + E \frac{\partial f}{\partial u_0} + F \frac{\partial f}{\partial \theta_0} + R_{23} \sin \theta_0 \frac{\partial f}{\partial R_0} \right) \\ &+ \frac{1}{\lambda u_0^2} \frac{\partial}{\partial R_0} \left( R_{03} f + R_{13} \frac{\partial f}{\partial u_0} + R_{23} \frac{\partial f}{\partial \theta_0} + R_{33} \frac{\partial f}{\partial R_0} \right) \end{aligned}$$

where

$$\begin{aligned} R_{03} &= \lambda \left\langle A_c \frac{\partial R_0}{\partial u} + \frac{D_c}{\sin \theta} \frac{\partial R_0}{\partial \theta} \right\rangle; \quad R_{13} = \lambda \left\langle B_c \frac{\partial R_0}{\partial u} + C_c \frac{\partial R_0}{\partial \theta} \right\rangle \\ R_{23} &= \lambda \left\langle B_c \left( \frac{\partial \theta_0}{\partial u} \right) \left( \frac{\partial R_0}{\partial u} \right) + C_c \left( \frac{\partial \theta_0}{\partial u} \frac{\partial R_0}{\partial \theta} + \frac{\partial R_0}{\partial u} \frac{\partial \theta_0}{\partial \theta} \right) + \frac{F_c}{\sin \theta} \left( \frac{\partial \theta_0}{\partial \theta} \right) \left( \frac{\partial R_0}{\partial \theta} \right) \right\rangle \\ R_{33} &= \lambda \left\langle B_c \left( \frac{\partial R_0}{\partial u} \right)^2 + 2 C_c \frac{\partial R_0}{\partial u} \frac{\partial R_0}{\partial \theta} + \frac{F_c}{\sin \theta} \left( \frac{\partial R_0}{\partial \theta} \right)^2 \right\rangle \end{aligned}$$

Here,  $\partial R_0/\partial u$ ,  $\partial \theta_0/\partial u$ ,  $\partial R_0/\partial \theta$ ,  $\partial \theta_0/\partial \theta$  are the transformation coefficients from a local point along orbit  $(u, \theta, R, Z)$  to the midplane, and  $\lambda = J/(u_0^2 \sin \theta_0)$  being the normalized FOW-Jacobian. The ‘‘radial’’ coefficients  $R_{03}$ ,  $R_{13}$ ,  $R_{23}$ ,  $R_{33}$  are expressed through the local collisional coefficients  $A_c, B_c, C_c, D_c, E_c, F_c$  [2]. These radial coefficients are absent in ZOW or Hybrid-FOW version. They give rise to the neoclassical bootstrap current and radial diffusion and pinches due to orbit modifications by collisions. Velocity diffusion terms  $B, C, E, F$  are not completely new – they are also present (in ZOW form) in the Hybrid-FOW version. Here, they are revised to include transformation coefficients:

$$\begin{aligned} B &= \lambda \langle B_c \rangle, \quad C = \lambda \langle B_c \partial \theta_0 / \partial u + C_c \partial \theta_0 / \partial \theta \rangle, \quad E = \lambda \sin \theta_0 \langle B_c \partial \theta_0 / \partial u + C_c \partial \theta_0 / \partial \theta \rangle, \\ F &= \lambda \sin \theta_0 \langle B_c (\partial \theta_0 / \partial u)^2 + 2 C_c (\partial \theta_0 / \partial u) (\partial \theta_0 / \partial \theta) + (F_c / \sin \theta) (\partial \theta_0 / \partial \theta)^2 \rangle. \end{aligned}$$

Similar expressions can be written for the quasilinear RF diffusion operator.

The collisional drag coefficients are also modified:

$$A = \lambda \langle A_c \rangle, \quad D = \lambda \sin \theta_0 \langle A_c \partial \theta_0 / \partial u + (D_c / \sin \theta) \partial \theta_0 / \partial \theta \rangle.$$

Note that in ZOW version, only  $\partial \theta_0 / \partial \theta$  transformation coefficient is non-zero. Collisional operator is averaged along each orbit in  $(u_0, \theta_0, R_0)$ -space. Fully non-linear, that is, self-consistent local collisional coefficients [11] are implemented in CQL3D.

The above expressions exhibit the basic physics of FOW neoclassical transport: the collision/RF velocity diffusion leads to scattering in COM space at each point along the orbit, weighted by the dependence of the COM on local velocity,  $\partial I_i / \partial \mathbf{u}$ , and multiplied by the local collision and RF coefficients. We emphasize that this formulation of neoclassical transport applies to the full g.c. particle orbits in velocity space, with no assumption, as is the usual neoclassical theory, that g.c. orbits are small compared to the plasma radius. Moreover, the radial electric field is amenable to this treatment. We expect that examination of the individual particle flows in COM space will provide additional insight into neoclassical transport, beyond perhaps what is obscured by the distribution function averaging in moment theory.

One of the main challenges in development of the Full-FOW version is the internal boundary conditions (IBC). In the ZOW version, the IBCs “connects” the two borders of the trapped-passing cone (dashed lines in Fig. 2). When the largest trapped particle (the “pinch” orbit) is scattered by collisions in pitch-angle, it can become either a co-passing or a counter-passing particle. The IBCs are formulated in such a way that the total flux of particles across the two borders of the trapped-passing cone is zero, and the flux at the trapped side of each border is same, as it describes the same trapped particle. An important simplification in ZOW case is that the trapped-passing borders are straight lines, and that each IBC connects two borders at one flux surface. In the Full-FOW case, the pinch orbit crosses the midplane at different radii, hence, the IBCs should connect the fluxes at different radial grid points. As the development of the IBCs is still in progress, here we provide results of initial test for the Full-FOW model without IBCs.

The test is performed for the NSTX conditions without NBI or RF heating;  $D^+$  ions at  $T_i=1.27$  keV,  $E = 0-200$  keV energy range in simulations. The main purpose of the test is to compare the Full-FOW version with the Hybrid-FOW version. The first column in Fig. 3 corresponds to the Hybrid-FOW version. It shows the local distribution function at three midplane points; it is reconstructed from solution, which is simply a Maxwellian distribution in this test case. The dashed lines represent different boundaries; they are found from analysis of  $(\mu, p_\phi)$  space, for each  $u$ -level. The red lines mark the trapped-passing boundaries that are similar to ZOW-case boundaries. The bold magenta line marks the pitch angles for stagnation orbits (dot-like orbits). The orbits in near proximity of the stagnation line are passing orbits; the boundaries where they exist are shown with blue lines (one of them is always  $\theta_0 = \pi/2$ ). Black lines are related to the loss cone borders.

The second column in Fig. 3 shows the solution of FPE obtained with the Full-FOW version.

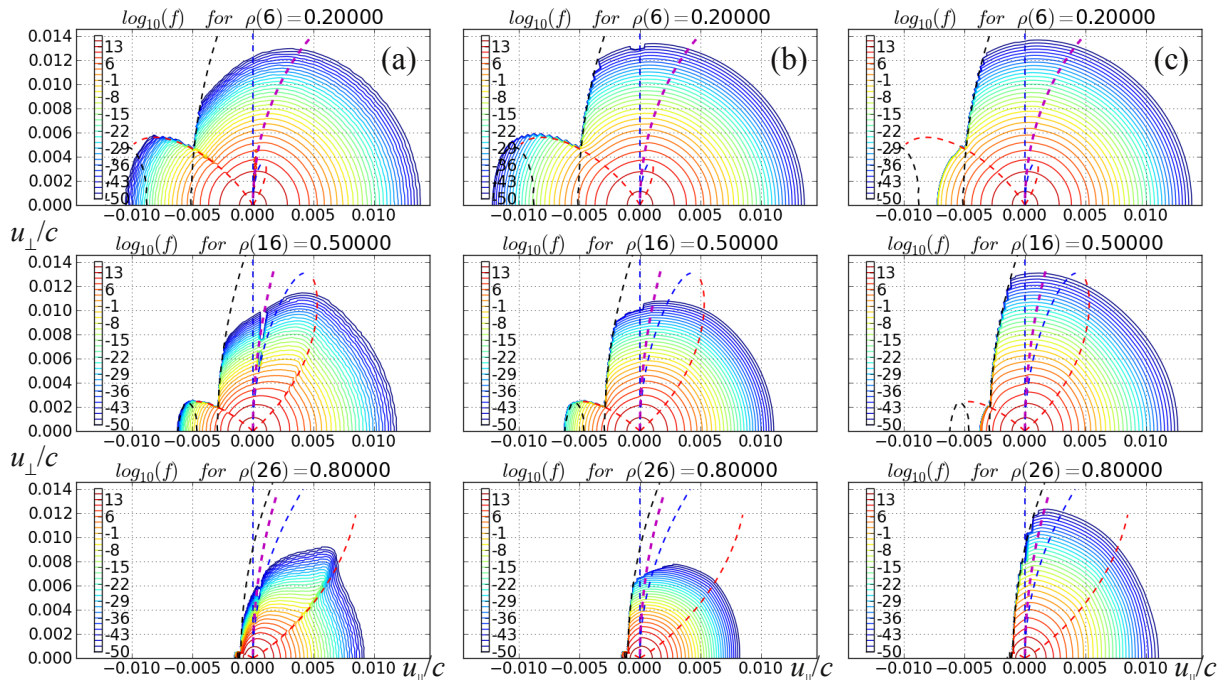


FIG. 3. Column (a) – reconstructed  $f_{loc}$  for the Hybrid-FOW run; (b) – solution obtained in the Full-FOW run without radial transport; (c) – Full-FOW run with radial transport.

The radial terms  $R_{03}$ ,  $R_{13}$ ,  $R_{23}$ ,  $R_{33}$  were not added in this run, so there is no radial transport in this case; the velocity diffusion and drag terms included all transformation coefficients as described above. It is seen that the distribution function in this run looks similar to that obtained with the Hybrid-FOW run. One noticeable difference is the presence of a “ridge” formed at the lower and upper trapped-passing boundaries (red dashed lines) in the Hybrid-FOW run. We believe that such “ridge” will also be formed in the Full-FOW runs when the IBCs are added into the code. The third column in Fig. 3 shows the results from the Full-FOW run with the radial transport enabled. In this run, a high-energy tail develops at  $\rho > 0.4$  that indicates to a radial transport of energetic ions from plasma core to the edge. Another new feature is a lack of counter-passing ions, next to the loss-cone. It appears that the rate of scattering of counter-passing particles into the loss cone, and additional radial transport of these particles, became higher than the rate at which particles are replenished from lower

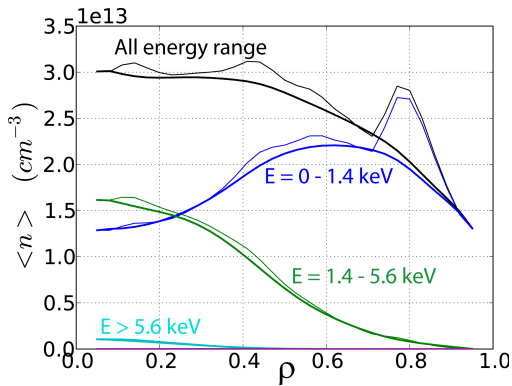


FIG. 4. Change of density profile in Full-FOW run with radial transport. Thin lines – at  $t = 0$ , bold lines – at  $t = 20 \text{ ms}$ .

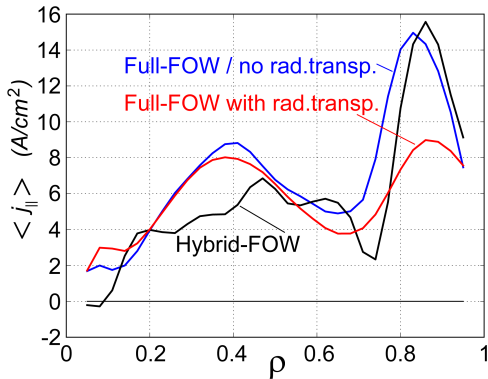


FIG. 5. Current density profiles in Hybrid-FOW and Full-FOW runs.

energies. It is also a possibility that a numerical instability develops in that velocity range; this is a subject for further investigation.

Additionally, Fig. 4 shows how the density profile of ions was changed in the Full-FOW run with radial transport. The initial profile was setup to have an initial “bump” at  $\rho \cong 0.8$ . It is seen that at  $t = 20 \text{ ms}$ , this “bump” has fully diffused out, and this change occurs mostly due to the thermal ions in the 0-1.4 keV energy range. Thus, the radial terms induced transport in both the high-energy range, as seen in Fig. 3(c), and in the thermal-energy particles.

Another focus of interest is the plasma current calculations. Fig. 5 shows the current profiles obtained in the three runs discussed here. The current profile in the Hybrid-FOW run is based on the reconstructed local distribution, as that shown in Fig. 3(a). Most part of this current is due to the loss cone. The figure also shows profiles for the Full-FOW runs with/without radial transport. The magnitude of the current reasonably agrees in all three cases, although the results in the Full-FOW runs cannot be accurate before the IBCs are applied.

In a summary, for high-energy diagnostics, the Hybrid-FOW model seems to capture the most of FOW effects. It is relatively simple, robust and almost as fast as the original ZOW version. It lacks the neoclassical transport, but a model radial transport can be used, same as in the CQL3D-ZOW version. The initial tests for the Full-FOW version show reasonable results; the internal boundary condition has yet to be added.

*Research supported by USDOE Contracts DE-FC02-01ER54649, DE-FG02-04ER54744, and DE-SC0000614.*

## REFERENCES

- [1] HARVEY, R.W., MCCOY, M.G., “The CQL3D F-P Code”, IAEA TCM, Montreal (1992).
- [2] HARVEY, R.W., MCCOY, M.G., “CQL3D Manual”, <http://www.compxco.com/cql3d>
- [3] EGEDAL, J., “Drift orbit topology of fast ions in tokamaks”, Nucl. Fusion **40** (2000) 1597.
- [4] LIU, D., et al., Plasma Phys. Control. Fusion **52** (2010) 025006.
- [5] HARVEY, R. W., PETROV, YU. V., LIU, D., HEIDBRINK, W. W., TAYLOR, G., BONOLI, P. T., “Temporal Dynamics of NSTX NBI+HHFW Discharges using CQL3D-Hybrid-FOW”, Bulletin of 54<sup>th</sup> Annual Meeting APS/DPP 57 (2012) PP8.00020.
- [6] BERNSTEIN, I.B., MOLVIG, K., "Lagrangian formulation of neoclassical transport theory", Phys. Fluids **26** (1983) 1488.
- [7] KAUFMAN, A.N., “Quasilinear Diffusion of an Axisymmetric Toroidal Plasma”, Phys. Fluids **15** (1972) 1063.
- [8] KUPFER, K., "Fokker-Planck Formulation for RF Current Drive, Including Wave Driven Radial Transport", Proc. of IAEA TCM on FWCD in Reactor Scale Tokamaks, Arles (1991).
- [9] ERIKSSON, L-G., HELANDER, P., Phys. Plasmas **1** (1994) 308.
- [10] BRIZARD, A. J., DECKER, J., PEYSSON, Y., DUTHOIT, F. X., Phys. Plasmas **16** (2009) 102304.
- [11] ROSENBLUTH, M. N., MACDONALD, W. M., JUDD, D.L., Phys. Review **107** (1957) 1.